The effect of tidal flow directionality on tidal turbine performance characteristics

C. Frost[*], C.E. Morris, A. Mason-Jones, D.M. O'Doherty, T. O'Doherty

School of Engineering, Cardiff University, Queen's Buildings, The Parade, Cardiff, CF24 3AA, United Kingdom

ABSTRACT

With many Tidal Energy Conversion (TEC) devices at full scale prototype stage there are two distinct design groups for Horizontal Axis Tidal Turbines (HATTs). Devices with a yaw mechanism allowing the turbine to always face into the flow, and devices with blades that can rotate through 180° to harness a strongly bi-directional flow. As marine turbine technology verges on the realm of economic viability this paper reveals the performance of Cardiff University's concept tidal turbine with its support structure either upstream or downstream and with various proximities between the rotating plane of the turbine and its support stanchion. Through the use of validated Computational Fluid Dynamics (CFD) modelling this work shows the optimal proximity between rotor plane and stanchion as well as establishing, in the given context, the use of a yaw mechanism to be superior to a bi-directional system from a performance perspective.

© 2015 The Authors. Published by Elsevier Ltd. This is an open access article under the CC BY license (http://creativecommons.org/licenses/by/4.0/).

1. Introduction

Tidal stream technology is one of the most recent forms of renewable energy to be developed as it offers predictable and regular electrical generation at higher power densities than other renewable energy resources [1]. However tidal stream turbines (TSTs) are best utilised to exploit areas where the flow is constrained by land and seabed topography such as islands and straits [2], and the current is accelerated to greater than 2.5 m/s to make their deployment cost effective [3]. The Department of Trade and Industry report on the economic viability of a simple tidal stream energy capture device [4], and UK resource estimates from Black and Veatch [3] suggest that typical water depths at the suitable sites around the UK range between 25 and 40 m and that consequently the corresponding recommended rotor diameter is between 10 m and 20 m. Although the rotor should ideally be placed as high as possible in the water column, to maximise the available power, it is not always practical to locate them there due to shipping constraints. For, example, the rotational axis of any horizontal TST placed in the Severn Estuary would need to be located 10 m above the seabed in a 35 m depth [5].

Since the rotors are never placed in isolation, but are typically housed on a support structure, it is important not only to characterise the performance of the rotor, but also to fully understand the interaction of the support structure on the flow characteristics. However, little work has been published on the direct effect of a support structure on the performance of a TST, especially when the support structure is upstream of the blades, as could be the case for turbines operating in dual-direction tidal flows. Prior work, carried out by Mason-Jones et al., [6] initially investigated the effect of the stanchion geometry for a horizontal TST, positioned 2 hub diameters or 3.6 m downstream of the rotor, on the characteristic performance of a TST. Different cross-sectional geometries were used to study axial thrust loading on the stanchion. Five different cross-sectional geometries were tested with an additional model without any supporting structure to give baseline values. The effects of these different cross-sectional geometries on the axial thrust are shown in Fig. 1, with a uniform velocity of 3.086 m/s. Although a stanchion with an elliptical or hydrofoil cross-section could be argued to provide the optimal stanchion design, a circular stanchion would be easier to manufacture and as such the circular stanchion was proposed as the stanchion design, based on a compromise between the various factors. As such the circular stanchion geometry will be used in this study.

Experience and knowledge gained from the wind industry has shown that the supporting structure always interferes with the fluid flow around the turbine blades due to the so-called tower dam effect as the flow is retarded in front of the supporting structure [7]. When the rotor is upstream of the supporting structure, the effects are minimal. However, when the blades are downstream, or in the

---

* Corresponding author. Tel.: +44 (0)29 2087 5905; fax: +44 (0)29 2087 4597.
E-mail address: frostc1@cf.ac.uk (C. Frost).

Nomenclature

D	turbine diameter (m)
r	radial distance (m)
R	turbine radius (m)
λ	tip speed ratio
CFD	computation fluid dynamics
TST	tidal stream turbine
L_n	clearance distance between turbine and support structure (m)
ω	rotational velocity (rad/s)
V	free stream velocity (m/s)
R	turbine radius (m)
ρ	density (Kg/m^3)
P	power (w)
F	force (N)
T	torque (Nm)

utilised a Wortmann FX 63-137 profile, with a 33° twist from the blade root to the tip. In particular, the study was conducted to assess how the tidal interaction with the supporting structure affected the performance characteristics of the turbine (i.e. power, torque, thrust and axial bending moments) for various clearance distance, as well as when the turbine is arranged either upstream or downstream of the support structure.

2. CFD

2.1. Model specifications and parameters

In order to understand the fundamental interaction between a blade passing in front of or behind a stanchion, a 3D model was created to establish the flow characteristics. The 3D modelling first determined the effects of stanchion clearance distance on the operational performance characteristics of the TST using a series of steady-state CFD models. Secondly, a transient model was then studied to determine the time dependent variables for the turbine.

The steady-state and transient models consisted of a control volume as defined in Table 1. With the 10 m diameter turbine located 100 m downstream of the inlet and its axis of rotation 25 m below the surface. The turbine is supported by a 2.4 m diameter stanchion which penetrates the complete water column. The axial clearance distance between the back edge of the blade and the front of the stanchion varied between L_1, L_2 or L_3 which are 1.8 m, 2.8 m & 3.8 m respectively either upstream or downstream. For the remainder of this paper these terms will be used to describe the various cases, for example 'L$_1$ Upstream' would refer to the 1.8 m separation distance between the support structure and the upstream turbine. The L_1 value corresponds to the hub diameter of Cardiff University's turbine. Distances beyond L_3 were viewed as unviable because of the large bending moments that would be incurred, and are not presented in this paper.

The turbine was enclosed by a cylindrical domain which was axially aligned with it. The cylinder and turbine were subtracted from the outer rectangular control volume to form a rotating frame of reference (RFR) with a general grid interface (GGI) connection between the sea and turbine volumes. Conservation of all terms are preserved across the connection interface, however the interface allows centrifugal and Coriolis momentum terms to be computed and solves a rotating frame total energy equation as described in ANSYS guide [8]. This arises from pre-defining the angular velocity of the rotating domain which corresponds with each tip speed ratio (TSR). The steady state model is time independent and provides a
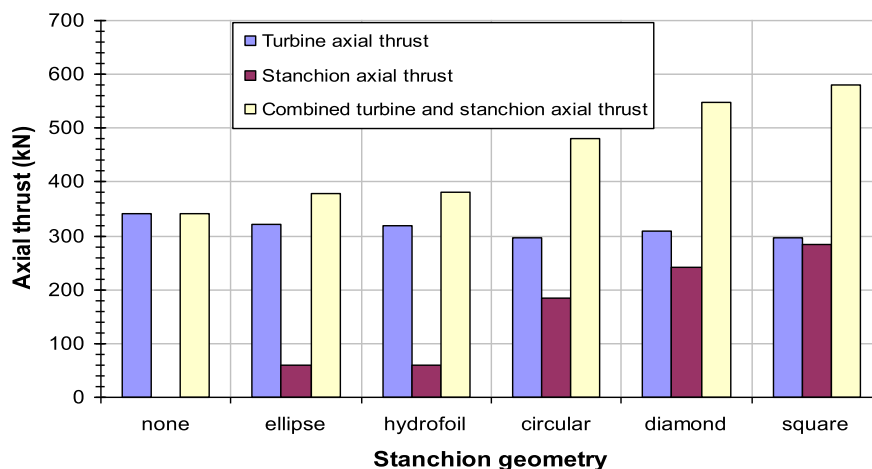
shadow of the supporting structure, the blades must pass through a sheltered area and this causes significant problems. One possible method to reduce the impact of this would be to increase the clearance distance between the turbine and support structure as this is expected to lessen the impact of the blockage on the turbine. There will be an economic and physical limit to the size of the clearance distance. Only by obtaining the characteristics of the turbine and flow for various clearance distances, however, can this benefit be defined. An alternative method of avoiding this situation would be to always face the blades into the free-stream velocity. This is reasonable within the wind industry where a yaw drive is simpler to incorporate and maintain. In the tidal stream environment, however, the flood and ebb tides would need to be considered to maximise the power generation. Although it may be technically feasible, to rotate the turbine to always face the oncoming flow, the added complexity and the harsh operating environment, let alone the increased capital costs and likely maintenance requirements, mean that the benefits from this option must be substantial. Hence it is important to fully understand the stanchion shadow effects on the turbine when upstream and downstream of a tidal stream turbine. As such a study using CFD has been undertaken to investigate the importance of turbine-stanchion proximity and arrangement on the performance of a 10 m diameter, 3 bladed horizontal axis tidal stream turbine which

Fig. 1. Effect of stanchion geometry on turbine power extraction and axial thrust.

Table 1
Domain specification.

Description	Specification [m]
Length	350
Breadth	50
Height	35

snapshot of performance; the transient model on the other hand provides the temporal performance of the turbine which is of much greater interest. Utilising both of these methods offers confidence and a comprehensive analysis of the cases.

The analysis parameters are as defined in Table 2 and were set the same for each case.

For the modelling ANSYS 14.5 was used with the Reynolds Averaged Navier—Stokes equations applied to relate the Reynolds Stresses to the mean velocity gradients. To close the equations the Shear Stress Transport (SST) was used as the viscous model.

The 'seabed' of the channel was modelled using the no-slip boundary condition, while zero-shear was applied to the side and surface boundaries. In order to maintain an economical computational model, free surface interaction between the water and air was not included.

The rectangular domain was sized to ensure the 10 m diameter turbine was fully isolated from any boundary effects. The centreline of the TST was positioned 10 m above the 'seabed' boundary leaving 25 m to the top surface boundary, in line with the requirements of a TST in the Severn Estuary [5].

Based on the turbine diameter, the radius of the circular stanchion was maintained with previous work as 1.2 m [9] and the stanchion penetrated the entire water column causing the stanchion to obstruct/interact with the whole of a blade when in a vertical position. The nacelle radius was specified as 0.9 m, the same size as the hub used in the previous studies [5,9]. Within the wind industry, the distance between the rotational plane of the turbine and the tower is generally kept to a minimum to avoid large bending moments [7]. Whilst this is certainly going to be the same for tidal turbines, the clearance in this study was varied between L_1 and L_3 for both the turbine upstream of the stanchion and for the turbine downstream of the stanchion. These cases will be used to investigate the effects of this clearance and arrangements on the performance characteristics of the TST. These cases are referred to as L_1 Upstream, L_1 Downstream, etc. in the rest of the paper.

In order to ensure the blade configuration was optimal for both the upstream and downstream conditions, each individual blade was rotated through 180° to face the flow so that the pitch angle was constant in both cases. It is worth noting at this point that in a real tidal cycle the downstream flow conditions may vary significantly to the upstream flow conditions, as for instance the flood phase of a tidal cycle may vary significantly from the ebb. For the case of this study however, they are assumed to be the same magnitude, but in the opposite direction relative to the turbine, as seen in Fig. 2.

Table 2
Analysis parameters.

Parameters	Values
Inlet velocity	3.086 m/s (6 knots)
Inlet turbulence intensity	5%
Sea water density	1025 kg/m^3
Sea water viscosity	0.00111 kg/ms
Reference pressure	0 Pa
Pressure outlet	0 Pa

2.2. Experimental validation

Validation testing was undertaken in the recirculating water flume at the University of Liverpool and has been reported in detail by Mason-Jones et al. [5] The flume utilises a 75 kW motor-driven axial-flow impeller to circulate 80,000 L of water. The water flows into the working section which is 3.7 m long by 1.4 m wide with a depth of 0.85 m. To ensure flow uniformity, a honeycomb and contraction guide vanes are used prior to the water entering the working section. The velocity upstream was known from detailed Laser Doppler Anemometry measurements in the flume which showed the free stream turbulence to be typically 3%, although it does vary with water speed. When the flume is used with its free surface configuration a contraction at the inlet ensures a mostly uniform velocity across the section with only thin boundary layers on the solid surfaces (~16 mm at the middle of the working section). To ensure there is no velocity deficit at the free surface, the surface flow, which is retarded, by the walls of the contraction, is re-energised using a thin jet which is added to the surface flow as it emerges from the contraction. For lab scale model TST testing, the working section was set to be an open flume, allowing the model turbine to be supported from above on a cross-beam.

The majority of model testing that has been reported to date has assumed that the power coefficient is independent of Reynolds number, although Batten et al. [10] do recognise the significance of Re in the selection of an 800 mm diameter TST. The important factor that has to be taken into account when testing a model turbine in the confines of a water flume is the blockage effect, whose correction is described in detail by others [11,12].

A typical set of result discussed by Mason-Jones et al. [5] revealed that the experimental data gave an error of ±5% when compared to the CFD data providing confidence in the predicted values. Whilst these validations were performed for a different study, the turbine geometry has been maintained. The same domain specifications as well as similar analysis parameters have also been utilised giving confidence in the validity of these results.

3. Results and discussion

3.1. Steady-state study

Considering the 3D steady-state study, it is possible to define the characteristics of the turbine such as the power coefficient (C_P), the torque coefficient (C_θ) and the thrust coefficient (C_T). By normalising these turbine characteristics they became directly comparable to the no stanchion datum set. These have been plotted for various TSR by varying the angular velocity (ω) and maintaining the inlet velocity and turbine diameter constant. The four parameters C_P, C_θ, C_T and λ have been defined in Equations (1)–(4) [5].

$$C_P = \frac{P}{\frac{1}{2}\rho A V^3} \tag{1}$$

$$C_\theta = \frac{T}{\frac{1}{2}\rho A R V^2} \tag{2}$$

$$C_T = \frac{F}{\frac{1}{2}\rho A V^2} \tag{3}$$

$$\lambda = \frac{\omega R}{V} \tag{4}$$

The converged solutions were interrogated for the forces acting on the turbine, specifically the blades. From the forces in the
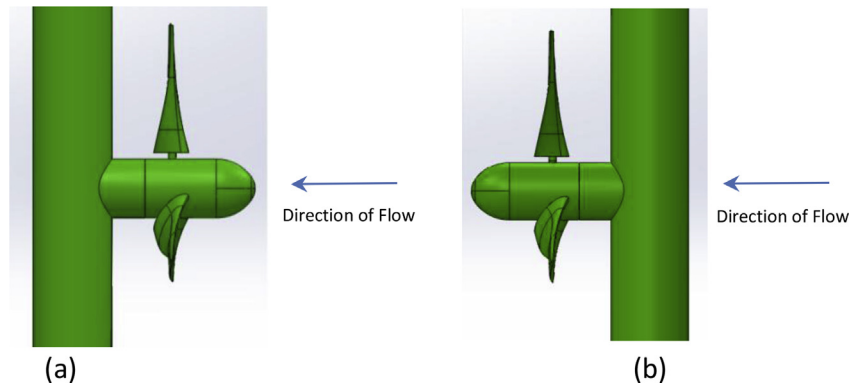
Fig. 2. Orientation of the TST; (a) for upstream conditions, (b) for downstream conditions.

appropriate axis the torque, thrust and power could be derived and used in Equations (1)–(4) to determine the coefficients.

The use of steady-state models was made as they are relatively in-expensive computationally and achieve a sufficient accuracy to provide generic performance criteria. The limitations of steady-state models are due to their removal of higher order 'time dependent' terms in the solver.

Fig. 3 is a graphical representation of the difference in C_P experienced when changing the direction of the flow. It can be clearly seen that the introduction of the stanchion, reduces the peak C_P and that for each of the stanchion clearance distances. Before considering the comparison between upstream and downstream conditions, the worst clearance distance for performance has been the small clearance distances offering at best 65% of the C_P of a no stanchion case. However larger clearance distances have achieved up to 89% C_P in relation to a no stanchion case. When including the comparison between upstream and downstream conditions, the C_P values for the upstream conditions are higher than those for the corresponding downstream conditions.

It can be said that C_P increases with increasing stanchion clearance for the upstream conditions. However for L_2 Downstream and L_3 Downstream, the C_P plots are almost identical though the clearance distance has increased. This may be a result of the wake recovery improving significantly from L_1 downstream to L_2 downstream, but not from L_2 to L_3 downstream. The same results are seen in the other characteristics of C_θ and C_T, Fig. 4 and Fig. 5 respectively. In the case of C_θ as expected the same order of performance applies as with C_P. As with C_T the lower the performance the better, and therefore the exact reverse order applies.

It should be noted that for the purpose of direct comparison, all plots for C_P, C_T & C_θ only contain results for the axial loading on the 3 blades and the hub, the stanchion is not included.

In light of these normalised curves, focus was taken on comparing the no stanchion case with the L_2 clearance distance. It can be seen from Fig. 6 that all of the L_2 curves are reduced by the presence of a stanchion in comparison to their no stanchion counterparts. The reduction in the thrust is a good thing however only if this reduction does not occur at the expense of the power and torque. The presence of a stanchion reduces the peak C_P value by over 7% to a value of 0.38, and reduces C_θ by 9.4% but C_T is only reduced by 5.9%. A slight shift in the location of the peak power is also seen causing the peak power to occur at a higher λ value. The C_P and C_θ curves also have a lesser gradient beyond the peak achieving greater values at higher λ values.

This is a steady state or time averaged solution where one blade was aligned with the stanchion at top dead centre (TDC) as previously seen in Fig. 2. For the given blade design, Fig. 6 also shows that as λ increases so does the axial loading, which plateaus as the turbine approaches the freewheeling velocity. This is because when the turbine is freewheeling, it offers most resistance to the flow. Operating at this condition should, be avoided for two reasons, the first being that since the torque becomes zero at the freewheeling velocity the power extracted would also become zero and secondly the axial load is highest in this condition. Beyond the freewheeling point C_T begins to drop as the turbine continues to be driven beyond the stall point. This issue arises due to the ANSYS code predefining the angular velocity in the analysis and it not obtained as an output of the model.
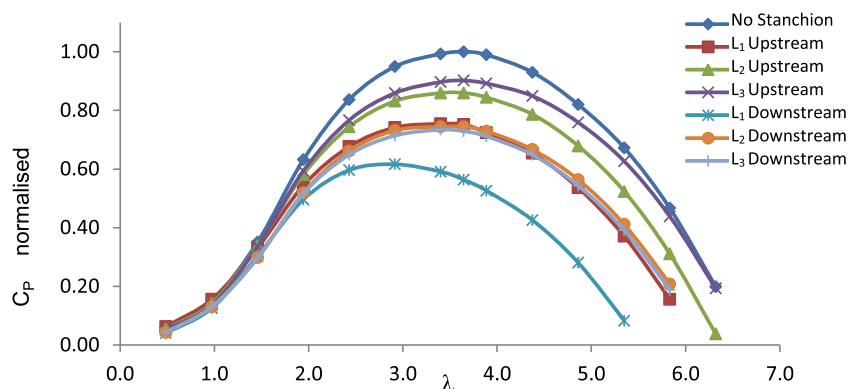

Fig. 3. Normalised C_p for upstream and downstream conditions at varying stanchion clearance distances.
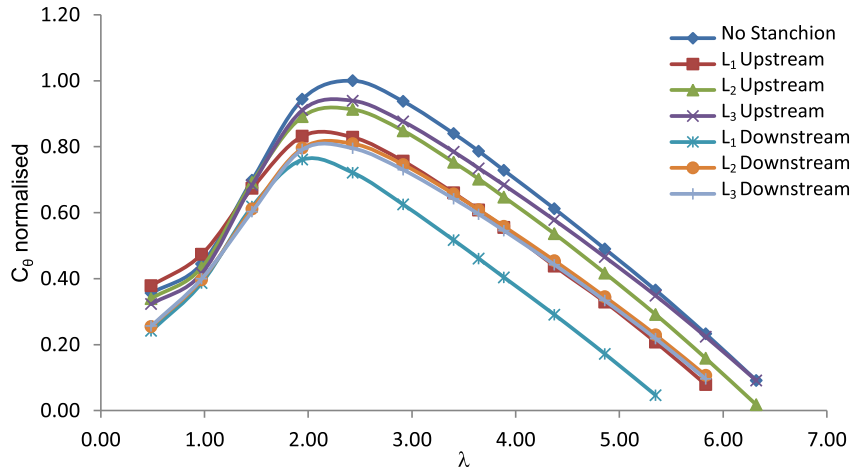
Fig. 4. Normalised C_θ for upstream and downstream conditions at varying stanchion clearance distances.

From the Steady-state study it has been established that the greater the clearance distance between rotor and stanchion the better the power and torque performance of the turbine. Also upstream flow conditions continually perform higher in these areas than their counterpart downstream flow conditions. Thrust however increases in magnitude with clearance distance, and for upstream flow conditions which is not desirable. The limitations of these results must be recognised as they are a time averaged solution, the effect of the stanchion during a single rotation and over a period of blades passing cannot be established from these results.

3.2. Transient study

To progress the understanding of turbine performance during rotation a transient model with the same parameters and geometry as the steady-state study was utilised. The transient models were analysed at a constant angular velocity of 2.1 rad/s ($\lambda = 3.40$), which is close to peak C_p value as determined from the steady-state study. For each transient study, the rotational cycle was considered as 240 timesteps. Fig. 7 shows the turbine position at every 20th timestep.

Fig. 8 shows the truncated C_P results for 720 timesteps or 3 complete rotational cycles where each trough represents one blade being in line with the stanchion while the peaks represent the position in the cycle where no blade is directly in front of the stanchion or in its shadow. It can be seen that there are larger fluctuations when the clearance distance is reduced for both the upstream and downstream cases. In the upstream case the amplitudes of fluctuations are small even at the distance of L_1. There is, however, a small reduction in the average C_P, as was seen in the steady-state models. The C_P values for the downstream case flow are particularly interesting. The average C_P values are virtually the same as each other, but reduced by around 9% in comparison to the upstream case flow values. What is very noticeable is that the amplitudes are highly magnified. It is also clear that the highest fluctuations are at a clearance of L_2, with only a small difference between the clearances of L_1 and L_3. This is possibly due to the flow between the blade and stanchion becoming more turbulent as the clearance increases from L_1 to L_2 and then stabilising as the clearance opens up further to the L_3.

Fig. 9 shows the results for the transient variations for C_T. What is clear is that the upstream conditions mimic those of the C_P curves, in as much as the fluctuations are small even at the smallest clearance distance. However, whilst the C_T curves for the downstream conditions also display high levels of fluctuations the amplitudes inversely reflect the clearance distances. That is the amplitudes increase as the clearance decreases. A positive to this though is that the average magnitude of the C_T is reduced when compared to the upstream conditions. Although the reduction in
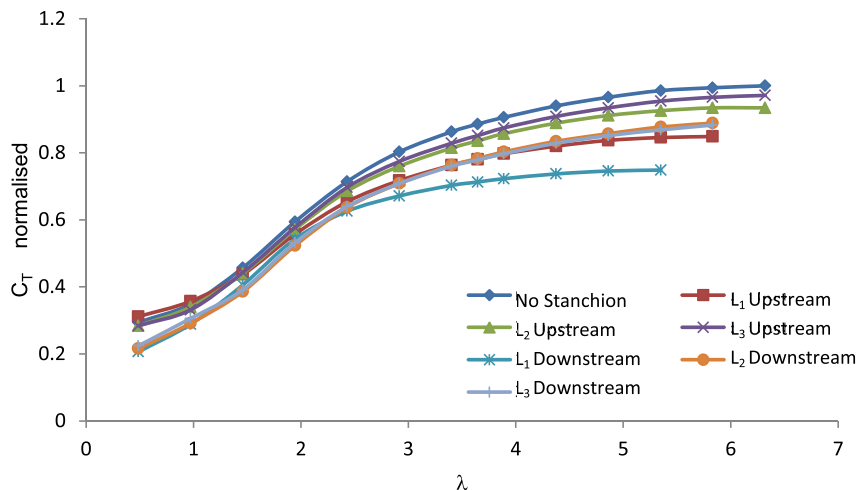

Fig. 5. Normalised C_T for upstream and downstream conditions at varying stanchion clearance distances.
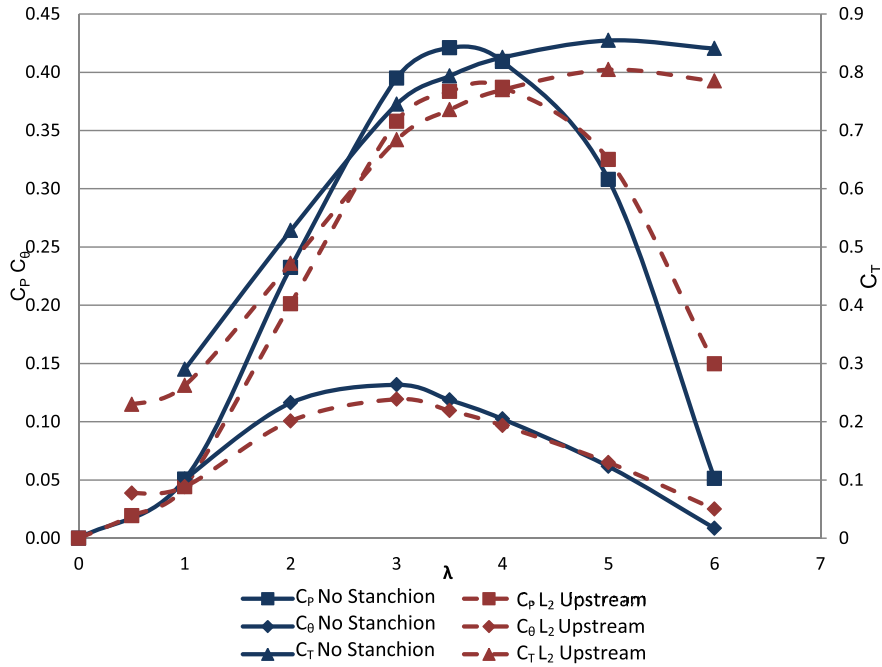
Fig. 6. Characteristics for a turbine with no stanchion and a turbine upstream of stanchion with clearance distance of L_2.

average C_T may be a positive outcome the greater amplitude of these fluctuations will result in the turbine blades pulsing over a rotational cycle. This will detrimentally harm the life of the turbine as it will lead to increased wear and fatigue issues. Thus the life of the device will be reduced.

Fig. 10 looks at the pitch and amplitude of the fluctuations in C_T and C_P over a third of a rotation for the downstream case. What is clear is that the curves are not symmetrical as the blade passes through the shadow of the stanchion. There is a sharp increase in the thrust and a more gradual drop as the blade passes out of the shadow. The shape of the C_T curve is reflected in the C_P curves with a rapid drop off of power as the blade passes through the shadow of the stanchion and a more gradual rise as the blade passes out of the shadow. In addition the peak values on both sets of curves are not coincident, such that the smaller the clearance the more delayed the lows and highs of the fluctuations. The cause for this

asymmetry in the performance characteristics as a blade passes the support structure can be identified through the velocity contour plot (Fig. 11) which was taken in the horizontal plane, 3 m above the axis of the turbine. As the blade passes the stanchion a low velocity region forms between the stanchion and the blade. The closer the blade is to the stanchion, the stronger this low velocity region attaches between them. This attachment as can be seen by the darker shades in Fig. 11 do not attach until the blade has almost passed the stanchion and remain attached until a distinct distance after the blade has passed beyond the stanchion. This may be the cause for the asymmetry in Fig. 10, as the blade remains de-powered for longer on exiting the region affected by the stanchion. The effects discussed are for a simple uniform flow condition.

By plotting the axial thrust applied to the centre of pressure of each blade on a polar plot, as seen in Fig. 12 with the polar co-ordinates in degrees from Blade 1 at Top Dead Centre (TDC), it is
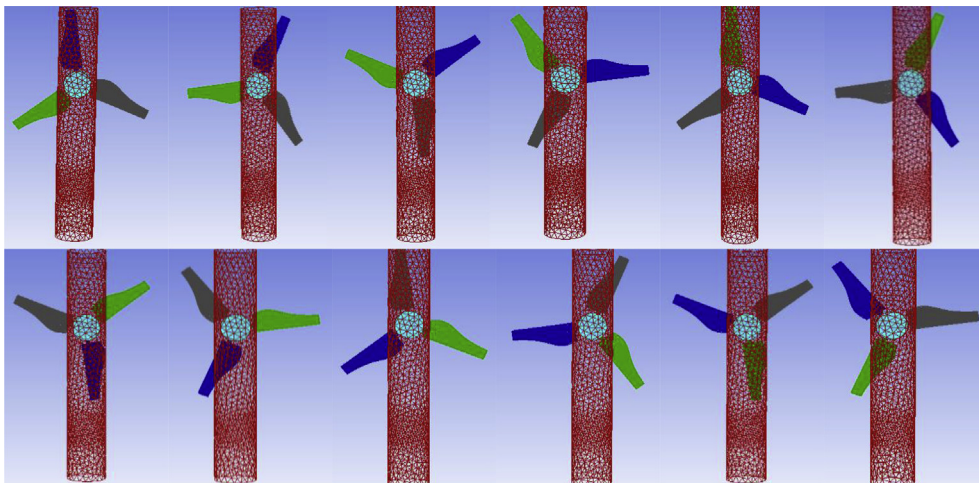

Fig. 7. The rotation sequence of the blades in a transient study.
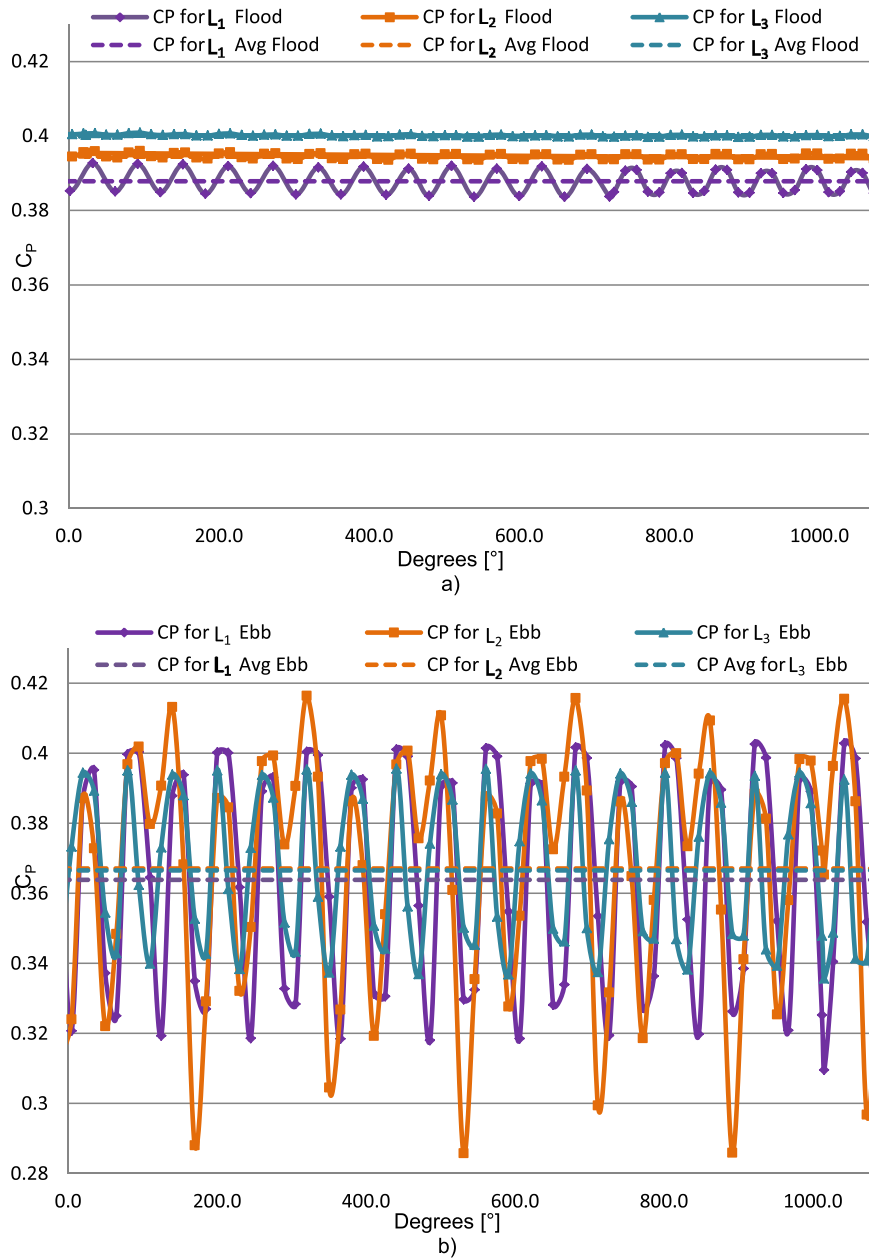
Fig. 8. C_p over 3 complete rotational cycles for a) Upstream and b) Downstream cases.

seen that each blade will experience 2 reductions in axial thrust per rotation. These reductions are the effects of the blade passing the stanchion at TDC and Bottom Dead Centre (BDC). For the complete turbine the thrust is reduced ever 60° relating to the number of blades and their frequency of passing the stanchion. By placing all of these plots on the same scale the significance of the drop in thrust are clearly seen. For the upstream case as proximity decreases the effect of the stanchion is lessened. For the downstream case on the other hand the change in proximity has much less effect on the drop the stanchion causes in axial thrust. The drop in thrust is much sharper in the downstream case as would be expected from what has been seen in Fig. 12. The flow has already been disrupted by the presence of the stanchion and has not had time to recover before encountering the blades. It therefore has a much lower velocity and hence imparts a much lower axial thrust.

Observing the total combined axial thrust experienced by the turbine as seen in Fig. 13 it is clear that the loads in the upstream

cases are much greater than in downstream cases, meaning the downstream cases are more desirable for reducing thrust. This benefit is outweighed however by the presence of highly fluctuating loads in the downstream cases. The troughs are again caused by low flow velocities due to stanchion disruption resulting in a lower thrust, making the higher but constant upstream conditions more desirable.

Previous study by Mason-Jones et al. [6] showed the presence of asymmetric loading and the compounded complexity with the presence of a stanchion. This work has been furthered by looking at the resultant axial bending moment that acts on the drive shaft and the angle at which that resultant bending moment acts. The axial thrust loads at the centre of pressure on each blade give rise to a bending moment about the x and y direction from the rotational axis of the turbine (Fig. 14).

When there is no stanchion present the resultant bending moment from the blades about the rotating axis is small but
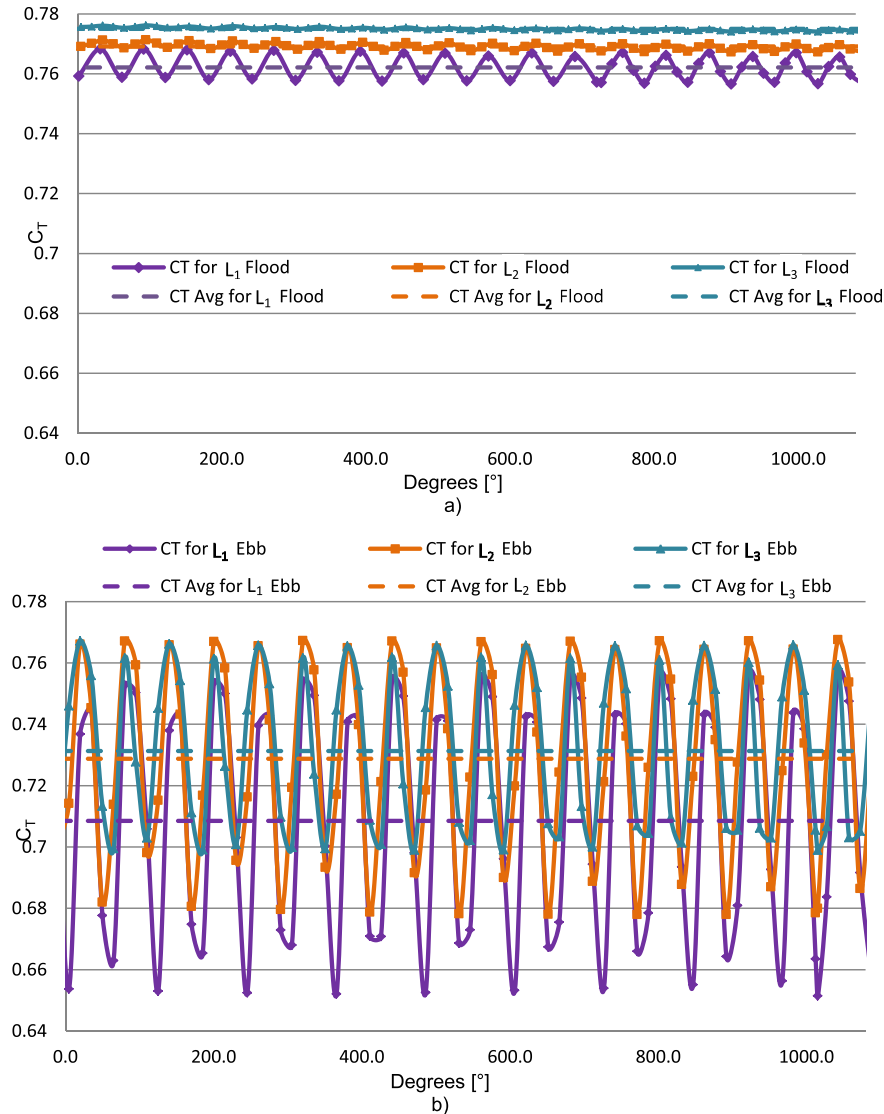
Fig. 9. C_T over 3 complete rotational cycles for a) Upstream and b) Downstream cases.

present as can be seen from Fig. 15. This slight inherent bending moment may come from the geometry of the blades however its magnitude is such that it is negligible in comparison to when there is a stanchion present.

The same procedure was performed for all clearance distances, the resultant axial bending moment and angle at which it is acting for the upstream cases can be seen in Fig. 16 and the same for the downstream cases in Fig. 17. The figures show non-symmetric loading is exerted on the drive shaft, resulting from the shadowing effect of the stanchion. Under the upstream cases, Fig. 16, it can be seen that the average axial bending moment reduces from ~38 kNm to ~12 kNm, as the clearance distance between the turbine and stanchion is increased from L_1 to L_3. There is also clear evidence that the amplitude of the bending moment, over the rotational cycle, reduces so mitigating some of the fatigue issues that would otherwise result. What can be deduced from this is that the peak bending moments occur when one blade is approximately in line with the stanchion, although there is a small increase in the lag the greater the increased separation. The minima in all cases occur at ~36° past the peak values. The direction at which the peak axial bending moment occurs for the distance L_1 and L_2 is at 120°

and the minima alternates between 160° and 340°. This is very different for the distance L_3, where the peak values have drifted from the 60° rotational position and the curve indicating the direction in which the axial bending moment is acting, has become more complicated. Unlike the previous 2 clearance distances, at L_3 there are three distinct peaks per 120° in comparison to two distinct peaks seen in the other separation distance. This is most likely due to the flow regime between the turbine and stanchion at this distance. What is obvious between all three cases is that the data repeats every 120° of rotation.

The thrust forces acting at the centre of pressure on the blades produce greater bending moments during the downstream case, Fig. 17, with a greater variation in magnitudes over the range of separation distances. At L_1 the average axial bending moment is ~70 kNm with a peak of ~150 kNm and a minimum of ~17 kNm. At the distance of L_2 the average has reduced to ~60 kNm with a peak of ~120 kNm and a minimum of ~12 kNm. At the distance of L_3 the average value has had only a small reduction to~58 kNm, with a peak value of ~106 kNm and a minima of ~9 kNm. The average magnitude of the bending moment is much greater than that of the upstream case, the increased clearance does show reduced
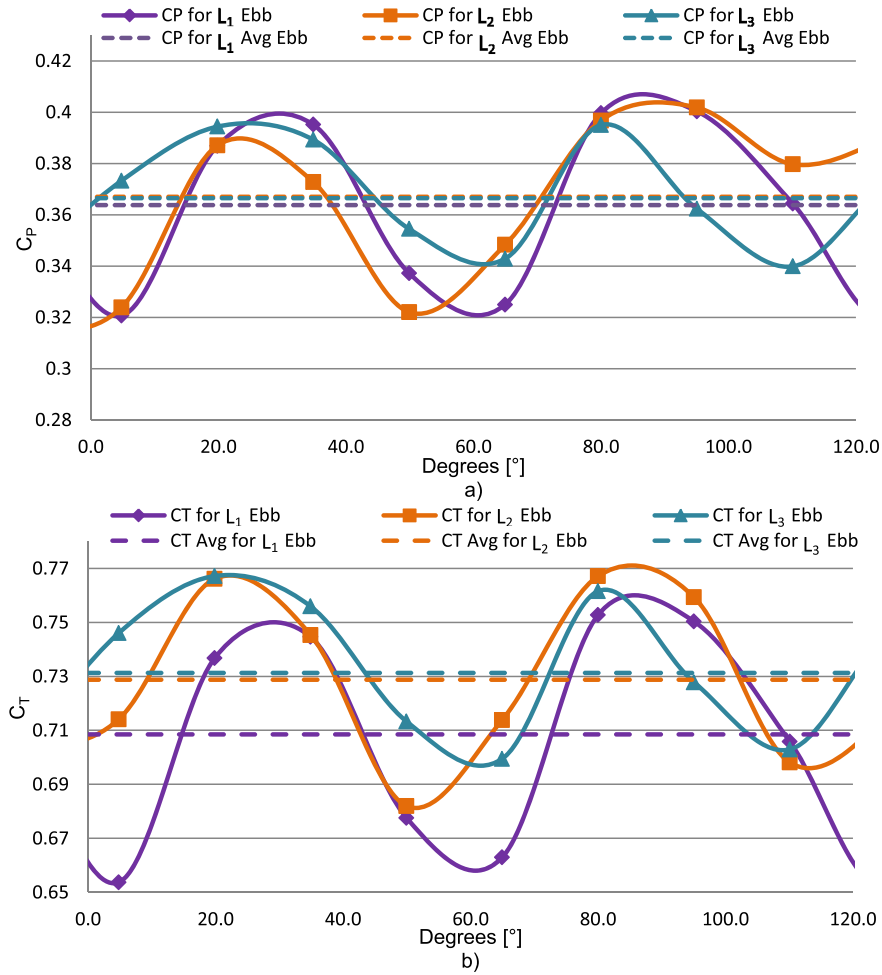
Fig. 10. Detail of the fluctuation in a) C_P and b) C_T as the blade rotates.

amplitude from ~130 kNm to ~100 kNm, but is still relatvely high. Similar to the upstream case the data repeats after every 120°. However unlike the upstream cases the direction in which the axial bending moment acts does become less complicated with an increase in the separation distance.

The presence of such significant axial bending moments as seen in Fig. 17 is undesirable due to its inevitable impact on the wear of

the turbine parts. Avoiding the transfer of these loads to the power generation will be important. Bearings along the drive shaft of the turbine will suffer significant fatigue issues from such loading. Resulting in shorter maintenance periods and increasing the cost per KWh on the turbine.

The transient study has shown the performance of the turbine during rotation. The fluctuations experienced in power, thrust and

Fig. 11. Velocity contours for L_1 upstream clearance at increasing timesteps.
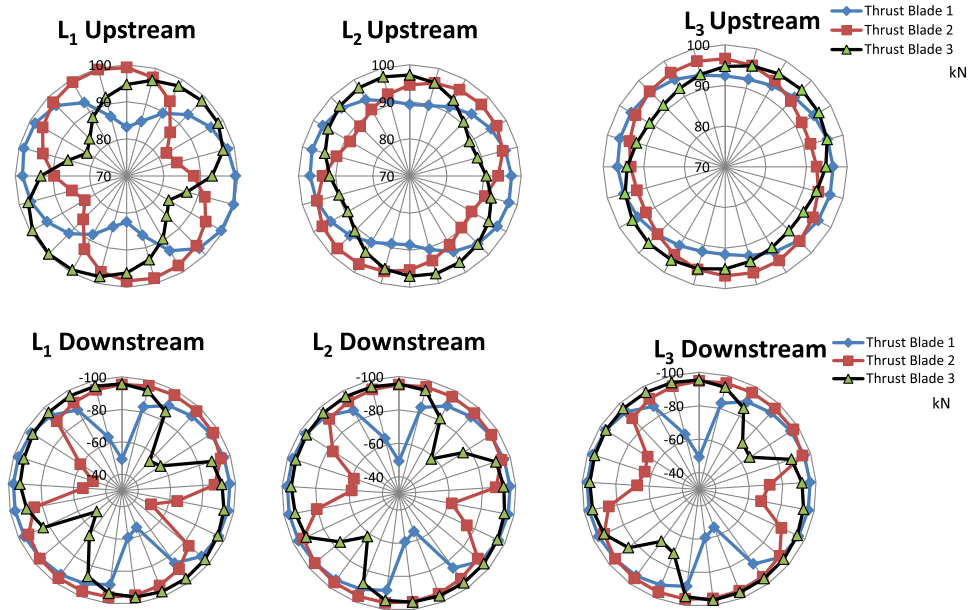
Fig. 12. Polar loading plots of axial thrust applied to the centre of pressure of the turbine blades over a complete rotational cycle for all three blades. Note the negative sign convention for the downstream plots comes from the setup of the transient models being in the opposite orientation to the upstream cases.
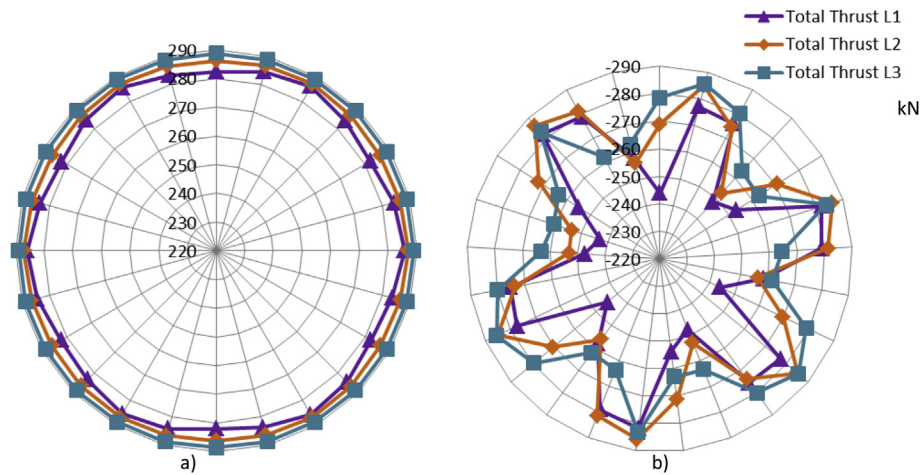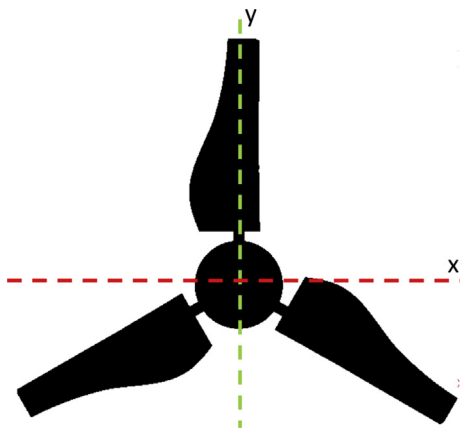

Fig. 13. Total axial thrust on the turbine from all 3 blades for a) Upstream and b) Downstream flows, over a complete rotational cycle. Note the negative sign convention for the downstream plots comes from the setup of the transient models being in the opposite orientation to the upstream cases.

Fig. 14. Axis for which bending moment are taken about.

axial bending moments have been established as a result of blade and stanchion interaction. The impact of this interaction is seen to be lessened with increased clearance distance and during the upstream cases. The agreement between steady-state and transient studies enables greater confidence in the results and with the issues raised.

4. Conclusion

One of the objectives of this paper was to determine whether a turbine should be configured to operate in a bi-directional manner. In this arrangement the turbine will experience upstream and downstream condition for each tidal cycle. However a turbine configured with a yawing mechanism would experience the equivalent of 2 upstream cases in one tidal cycle (assuming tidal symmetry). It has been shown by both the steady-state and transient results that the turbine in this scenario operates best in the
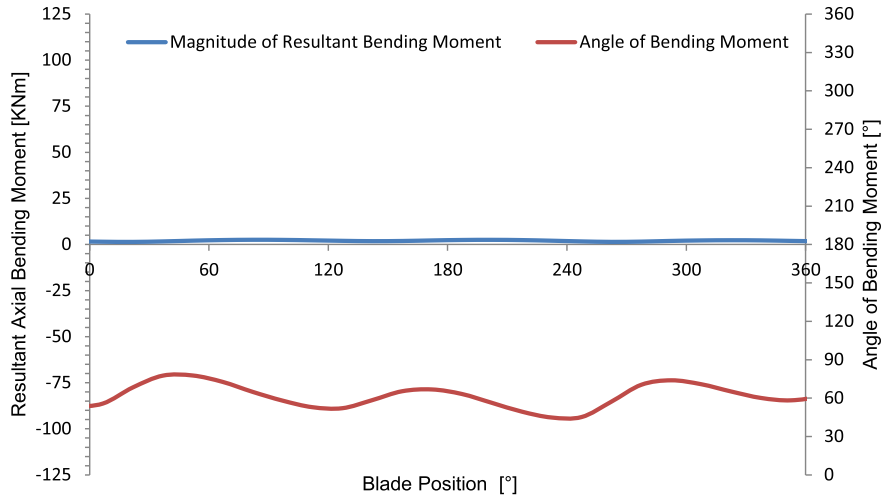
Fig. 15. Resultant bending moment over a rotational cycle of the turbine with no stanchion.
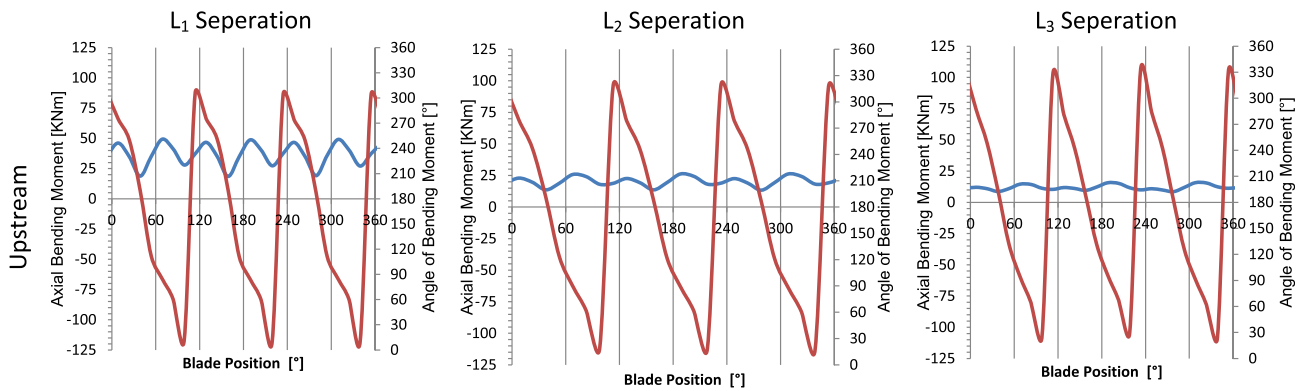

Fig. 16. Magnitude of resultant bending moments and angle acting on the drive shaft under upstream conditions.
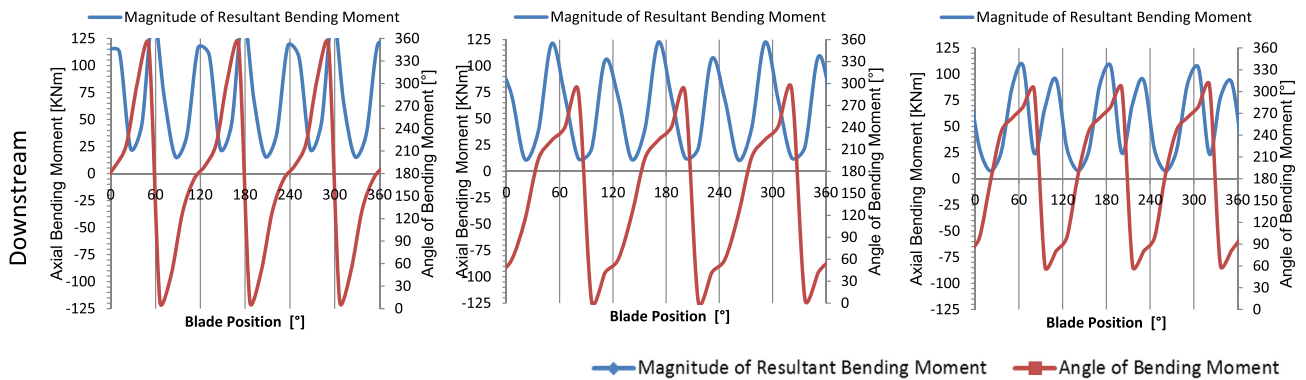

Fig. 17. Magnitude of resultant bending moments and angle acting on the drive shaft under downstream conditions.

upstream arrangement. What may be the most significant factor is the axial bending moment experienced by the turbine. As shown in the results, the downstream cases experiences peaks $10\times$ greater than the average moment for the upstream cases at the same clearance distance.

In conclusion then a yaw mechanism is beneficial to the performance and fatigue life of a turbine in this scenario. It must be mentioned however that there are alternative solutions emerging such as tethering the turbine and avoid the use of a stanchion altogether, such as that employed in the contra-rotating design at Strathclyde University [13].

The effects of clearance distance between the rotary plane of the turbine and the stanchion have also been presented. It has been shown that the greater the clearance distances the better the performance of the turbine. The performance of the turbine at clearance distance L_3 was the closest to optimal (no stanchion) conditions, as shown by steady-state study. The transient study revealed with greater clearance distance the less the amplitude of oscillation which is of significant benefit to power conditioning and fatigue life of the turbine. This supports the need for the turbine to be located as far from the structure as economically and mechanically viable. Hau suggests that the clearance distance for a wind

turbine should be a minimum of one tower diameter upstream, based on the flow field ahead of the tower and the need to keep the bending moments to a minimum [7]. This would agree with the case of Cardiff Universities turbine and chosen support structure, since the recommended clearance is between 2.8 m and 3.8 m, which is greater than the stanchion diameter of 2.4 m.

The study reported in this paper whilst being performed for both steady-state and transient models used ideal flow conditions. It is not unreasonable to extrapolate these findings to a more realistic velocity profile, with transient surging to realise that even a shaped support structure would still result in significant loadings, with high levels of oscillation. The variation in velocity across the face of the turbine [6] as well as its time dependent aspect will add further complexities to the loading. Whilst there may be capital costs in ensuring the whole turbine faces the flow, i.e. yaw mechanism, the extension to the turbine life could be significant enough to justify this. Other areas of interest would be to include true deflections experienced by the turbine blades and support structure. This would be achievable through the use of Fluid—Solid Interaction, FSI analysis. These methods will be implemented in future work and will greatly improve the models in attempting to achieve realistic at sea conditions.

Acknowledgements

References

[1] Bahaj AS, Myers L. Analytical estimates of the energy yield potential from the Alderney Race (Channel Islands) using marine current energy converters. Renew Energy 2004;29:1931—45.
[2] Fraenkel PL. Marine current turbines: pioneering the development of the marine kinetic energy converters. Proc IMechE 2006;221. Part A: J Power Energy.
[3] Black and Veatch. Tidal stream energy resource and technology summary report. Carbon Trust; 2005.
[4] DTI. Economic viability of a simple tidal stream energy capture device. 2007. DTI project No. TP/3/ERG/6/1/15527/REP URN 07/575.
[5] Mason-Jones A, O'Doherty DM, Morris CE, O'Doherty T, Byrne CB, Prickett PW, et al. Non-dimensional scaling of tidal stream turbines. Energy 2012;44: 820—9.
[6] Mason-Jones A, O'DOherty DM, Morris CE, O'Doherty T, et al. Influence of a velocity profile & support structure on tidal stream turbine performance. Renew Energy 2012;52(2013). ISSN: 0960-1481:23—30. http://dx.doi.org/10.1016/j.renene.2012.10.022.
[7] Hau E. Wind turbines: fundamentals, technologies, application, economics. 2nd ed. Germany: Springer; 2006.
[8] Ansys guide — Release 15.0 [accessed 15.12.14].
[9] Mason-Jones A. Performance assessment of a horizontal axis tidal turbine in a high velocity shear environment. PhD Thesis. Cardiff University; 2010.
[10] Batten WMJ, Bahaj AS, Molland AF, Chaplin JR. Experimentally validated numerical method for the hydrodynamic design of horizontal axis tidal turbines. Ocean Eng 2007;34(7). ISSN: 00298018:1013—20. http://dx.doi.org/10.1016/j.oceaneng.2006.04.008.
[11] Whelan JI, Graham JMR, Peiro J. A free-surface and blockage correction for tidal turbines. J Fluid Mech 2009;624:281—91.
[12] Chen TY, Liou LR. Blockage corrections in wind tunnel tests of small horizontal-axis wind turbines. Exp Therm Fluid Sci 2011;35(3):565—9.
[13] Clarke JA, Connor G, Grant A, Johnstone C, Ordonez-Sanchez SE, et al. Contra-rotating marine current turbines: single point tethered floating system — stability and performance EWTEC. 2009.